

An exact solution to the inverse problem of steady free-surface flow over topography

M. G. Blyth

^a*School of Mathematics University of East Anglia Norwich NR4 7TJ UK*

Abstract

A simple exact solution is presented to the inverse problem in steady, two-dimensional idealised flow over topography that seeks the bottom profile given knowledge of the free-surface data. Attention is focused on the case when a uniform stream flows over a localised obstacle, although the solution is not restricted to this case. The inverse problem is formulated as a Stieltjes integral equation which is solved exactly using a Fourier transform. The solution requires the analytic continuation of two real functions representing the surface speed and the angle between the surface velocity vector and the horizontal. Some example surface profiles and their corresponding bottom topographies are discussed. Although the solution requires the prescription of the surface as a function of the velocity potential, it is shown to closely resemble the corresponding profile in physical space, even for quite large surface displacements, while significant discrepancy occurs at the bottom. Inference of the bottom profile from discrete surface data is accomplished by way of polynomial interpolation and rational approximation in the complex plane for the sample case of a hydraulic fall.

1. Introduction

The study of idealised free-surface flow over topography has attracted the attention of researchers for many years. Much of this has been reserved for what we refer to as the forwards problem, which involves determining the surface profile given knowledge of the bottom topography. Considerable effort has been devoted to understanding the surface response in the presence of some localised topographic feature and the disruption that it provokes to an otherwise uniform stream. For example, flow over a semicircular obstacle was discussed by Forbes & Schwartz [1], flow over a semi-elliptical bump was examined by Forbes [2], and flow over a triangular obstruction was considered by Dias & Vanden-Broeck [3].

Typically in the aforementioned works a solution to the fully nonlinear forwards problem was obtained numerically using either a series truncation method, or else by a collocation method after first reformulating the governing equation in the fluid as an integral equation. King & Bloor [4] formulated the fully nonlinear problem in terms of an integral equation for the bottom angle (the angle between the tangent to the topography and the horizontal) and the fluid speed. Essentially the same formulation was later adopted by Binder *et al.* [5], who also categorised the flow over a localised obstacle into eleven basic flow types depending on the size of the Froude numbers upstream and downstream of the obstacle. The dimensionless Froude number, F , is defined by

$$F = \frac{U}{\sqrt{gH}}, \quad (1.1)$$

where U is the strength of the unobstructed flow, g is the acceleration due to gravity, and H is the undisturbed fluid depth. It provides a measure of the uniform flow speed

against the speed of small amplitude gravity waves on water of finite depth. Free surface flow over an obstacle is usefully divided into subcritical flow, for which $F < 1$ and which is typically characterised by a train of periodic waves downstream, and supercritical flow, for which $F > 1$ and which does not exhibit waves downstream.

From the opposite viewpoint the free surface profile is provided and the task is to solve for the corresponding bottom topography. It can be meaningfully referred to as the inverse problem since its formulation yields a Fredholm integral equation of the first kind, and such equations are well known to be ill-posed, a feature that is typical of inverse problems. In particular Tuck [6] noted that the inverse problem can be formulated as a Stieltjes integral equation. However, noting that the inversion of such equations is not straightforward, he did not proceed further with the analysis. Despite its practical importance, the inverse problem has received relatively little attention (see the review article by Sellier [7] for a summary). Other relevant studies for steady flow include those by Chardard *et al.* [8], Binder *et al.* [5], and Abdelrahman *et al.* [9].

In more recent work Robbins [10] and Robbins *et al.* [11] formulated the inverse problem for steady flow in terms of a Fredholm integral equation of the first kind, which was solved numerically. They showed that the ill-posedness could be mitigated by the careful use of a Truncated Singular Value Decomposition (TSVD). They also demonstrated how this method could be applied to handle noisy surface data via a statistical analysis. In the present work we address the same inverse problem for smooth surface data with a view to providing an exact solution. Working from a slightly different angle, we write the inverse problem in terms of a Stieltjes integral equation which is tackled analytically in a Fourier transform approach that mimics that deployed by Titchmarsh [12]. The solution necessitates the analytic continuation of the real functions representing the speed at the free surface and the surface angle, that is the angle between the surface tangent and the horizontal. From this the corresponding angle at the bottom can be extracted directly, and the bottom profile can then be constructed via a straightforward quadrature.

In practice understanding free-surface flow over bottom topography is relevant to a number of engineering applications including spillways and sluice gates. The recovery of river bed geometry is extremely important for building accurate flood inundation models (e.g. Neal *et al.* [13]). In a real-world flow complicating factors such as unsteadiness, turbulence, and noise are to be expected. Nevertheless, for the floodplain problem, Neal *et al.* [13] proposed the use of steady models to resolve the river channel bathymetry. Furthermore, steady results provide a useful benchmark for numerical simulations of more complex models.

In the next section we define the mathematical problem, and formulate the relevant Stieltjes integral equation for the bottom angle. In section 3 we show how the exact solution to the problem is constructed. Results for a number of sample surface profiles are presented and discussed in section 4. Finally, in section 5 we summarise and review our approach.

2. Problem formulation

We consider the steady, inviscid and irrotational flow of a fluid layer over a flat bottom that meets some topographic feature, as is sketched in Fig. 1. Far downstream the depth of the fluid layer approaches H , a constant, and the flow velocity approaches that of a uniform stream of strength U . It is convenient to eliminate the dimensions from the problem using H and U as the characteristic length and velocity scales, respectively.

Working in dimensionless variables the flow is described in terms of an analytic complex potential $w(z) = \phi(x, y) + i\psi(x, y)$, where $z = x + iy$, and ϕ and ψ are the

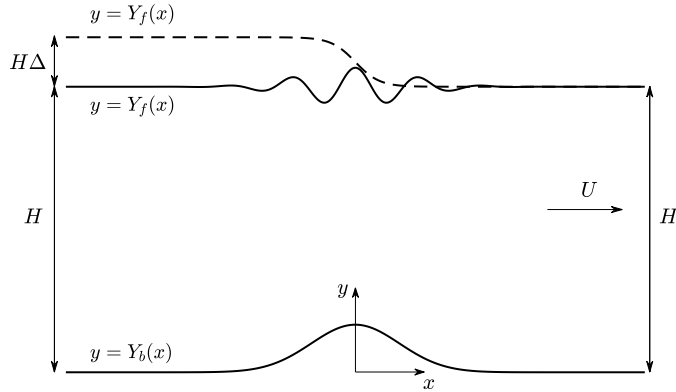


Figure 1: Sketch of the flow configuration. The flow, which is from left to right, approaches a uniform stream of strength U and depth H far downstream. A flow for which the surface approaches the same level both upstream and downstream is shown with a solid line. A hydraulic fall, for which the surface level drops downstream by an amount $H\Delta$, is shown with a dashed line.

velocity potential and stream function, respectively. The velocity potential in the fluid satisfies Laplace's equation

$$\nabla^2 \phi = 0. \quad (2.1)$$

The free surface corresponds to a streamline of the flow on which ψ is constant. The kinematic condition at the bottom requires that

$$v - u \frac{dY_b}{dx} = 0 \quad (2.2)$$

on $y = Y_b(x)$, where $Y_b(x)$ describes the shape of the topography, and where u and v are the dimensionless velocity components in the x and y directions, respectively. The dynamic boundary condition at the free surface, located at $y = Y_f(x)$, follows from Bernoulli's equation and is given by

$$\frac{1}{2}(u^2 + v^2) + \frac{\eta}{F^2} = \frac{1}{2}. \quad (2.3)$$

Here η is the displacement of the surface from the undisturbed downstream level. In writing down (2.3) we have used the fact that the flow approaches a uniform stream in the far field, so that $u^2 + v^2 \rightarrow 1$ and $\eta \rightarrow 0$ as $x \rightarrow \infty$.

We describe the complex potential $w(z)$ for the flow in terms of an analytic function $\tau(x, y) - i\theta(x, y)$, writing (e.g. Stoker [14])

$$\frac{dw}{dz} = u - iv = e^{\tau - i\theta}, \quad (2.4)$$

where $\tau = \ln(u^2 + v^2)$ and θ is the angle between the tangent to a streamline and the horizontal. Making use of Cauchy's integral formula, Binder *et al.* [5] derived the integral equation

$$\int_0^\infty \frac{g(\alpha')}{\alpha' + \alpha} d\alpha' = G(\alpha), \quad (2.5)$$

where $\alpha = \exp(\pi\phi)$, and $g(\alpha) = \pi^{-1}\theta_b(\alpha)$. We recognise (2.5) as a Stieltjes integral equation (e.g. Titchmarsh [12]). The forcing function is

$$G(\alpha) = \frac{1}{\pi} \int_0^\infty \frac{\theta_f(\alpha')}{\alpha' - \alpha} d\alpha' - \tau_f(\alpha). \quad (2.6)$$

A subscript f has been used to indicate a variable evaluated at the free surface. Similarly a subscript b indicates a value at the bottom.

3. Exact solution

The Stieltjes equation (2.5) is to be solved for g assuming that G is known; that is we aim to solve for θ_b with the surface data given. Since $y_f(\phi) = 1 + \eta(\phi)$, and following Robbins [10], we can rearrange the dynamic boundary condition (2.3) to give

$$\tau_f = \frac{1}{2} \ln \left(1 - \frac{2}{F^2} \eta \right). \quad (3.1)$$

Then $\theta_f(\phi)$ can be computed using the second of the relations

$$\frac{dx_f}{d\phi} = e^{-\tau_f} \cos \theta_f, \quad \frac{dy_f}{d\phi} = e^{-\tau_f} \sin \theta_f, \quad (3.2)$$

where $(x_f(\phi), y_f(\phi))$ describes the location of a point on the free surface. These relations follow from (2.4) on noting that $dz/dw = 1/(dw/dz)$. Once the inverse problem is solved the topography profile may be determined by integrating the relations

$$\frac{dx_b}{d\phi} = e^{-\tau_b} \cos \theta_b, \quad \frac{dy_b}{d\phi} = e^{-\tau_b} \sin \theta_b, \quad (3.3)$$

where $(x_b(\phi), y_b(\phi))$ describes the location of a point on the bottom.

The inverse problem just stated was formulated and solved numerically by Robbins [10] and Robbins *et al.* [11] using a numerical approach. The purpose of the present work is to provide an exact solution to the problem and to use it to compare with the numerical results. We solve (2.5) using a Fourier transform. Following Titchmarsh [12] we first introduce the new independent variable $\xi = \pi\phi = \ln \alpha$ and write

$$e^{\xi/2} \tau_f = t(\xi), \quad e^{\xi/2} \theta_b = b(\xi), \quad e^{\xi/2} \theta_f = f(\xi), \quad (3.4)$$

so that the task now is to determine $b(\xi)$ given knowledge of $f(\xi)$. In particular (2.5) becomes

$$\int_{-\infty}^{\infty} \frac{b(u)}{\cosh[\frac{1}{2}(\xi - u)]} du = -R(\xi), \quad (3.5)$$

where $R(\xi) = I(\xi) + 2\pi t(\xi)$, with

$$I(\xi) = \int_{-\infty}^{\infty} \frac{f(u)}{\sinh[\frac{1}{2}(\xi - u)]} du. \quad (3.6)$$

To proceed we take the Fourier transform of (3.5). To help with this step we note the following Fourier transforms

$$\int_{-\infty}^{\infty} \operatorname{sech}(\pi\xi/\mu) e^{ik\xi} d\xi = \mu \operatorname{sech}(\frac{1}{2}k\mu), \quad \int_{-\infty}^{\infty} \operatorname{cosech}(\pi\xi/\mu) e^{ik\xi} = i\mu \tanh(\frac{1}{2}k\mu)$$

for constant $\mu > 0$ and Fourier symbol k (see Bateman *et al.* [15] and Ablowitz & Clarkson [16], respectively). Using the convolution theorem and rearranging we obtain

$$\hat{b} = -i \sinh(\pi k) \hat{f}(k) - \cosh(\pi k) \hat{t}(k), \quad (3.7)$$

where a caret indicates a Fourier transform. Inverting the transform, we find that

$$b(\xi) = \frac{1}{4\pi} \int_{-\infty}^{\infty} \left(e^{-ik(\xi-i\pi)} - e^{-ik(\xi+i\pi)} \right) \hat{t}(k) - \left(e^{-ik(\xi+i\pi)} + e^{-ik(\xi-i\pi)} \right) \hat{f}(k) dk. \quad (3.8)$$

Reverting to the original variables using (3.4) we obtain the exact solution to the inverse problem,

$$\theta_b(\xi) = \frac{1}{2} \left(\theta_f(\xi + i\pi) + \theta_f(\xi - i\pi) \right) - \frac{1}{2} i \left(\tau_f(\xi + i\pi) - \tau_f(\xi - i\pi) \right). \quad (3.9)$$

Formula (3.10) requires the analytic continuation of the functions $\theta_f(\xi)$ and $\tau_f(\xi)$ off the real ξ line and into the strip $\mathcal{D} = \{-\pi \leq \text{Im} \xi \leq \pi\}$. Titchmarsh [12] showed that if $R(\xi)$ is analytic in \mathcal{D} and if $\int_{-\infty}^{\infty} |R(\xi + i\zeta)|^2 d\xi$ is bounded for real ξ and for $-\pi < \zeta < \pi$, then $b(\xi) \in L_2(-\infty, \infty)$. Evidently $R(\xi)$ is not analytic in \mathcal{D} if $t(\xi)$ has a singularity in \mathcal{D} . If $f(\xi)$ has a singularity in \mathcal{D} but is analytic in a narrower strip $-\lambda < \text{Im} \xi < \lambda$ for some $\lambda < \pi$, then its Fourier transform $\hat{f} \sim c_{\mp} \exp(\mp \lambda \text{Re} k)$ as $\text{Re} k \rightarrow \pm \infty$ [12, Theorem 26]. But $\hat{I}(k) = 2\pi i \tanh(\pi k) \hat{f}(k)$ so that \hat{I} and \hat{f} decay at the same rate for large $\text{Re} k$, and hence the analyticity of $I(\xi)$ is confined to the same narrower strip within \mathcal{D} . In summary, the presence of singularities of $t(\xi)$ and $f(\xi)$, and hence of $\tau_f(\xi)$ and $\theta_f(\xi)$, inside \mathcal{D} is important and we shall therefore pay particular attention to these in the ensuing discussion.

Assuming analyticity in \mathcal{D} it is straightforward to show that the real and imaginary parts of the analytically continued functions τ_f , θ_f are, respectively, symmetric and antisymmetric about the real axis. It follows that (3.9) reduces to the compact form

$$\theta_b(\xi) = \text{Im}[\tau_f(\xi + i\pi) + i\theta_f(\xi + i\pi)]. \quad (3.10)$$

If the free surface is perfectly flat then $\theta_f(\xi) \equiv 0$ and $\tau_f(\xi) \equiv 0$. The analytic extension of both of these functions is zero everywhere in the complex plane, and hence it follows from (3.10) that $\theta_b(\xi) \equiv 0$ and the bottom must necessarily also be flat (Robbins *et al.* [11] established the same result via a different argument). It also follows from (3.10) that if the free surface disturbance $\eta(\xi)$ is even about $\xi = 0$, so that $\text{Im}[\tau_f(\xi + i\pi)]$ and $\text{Re}[\theta_f(\xi + i\pi)]$ are both odd, then $y_b(\xi)$ is necessarily even, and hence the even parity of the bottom profile follows that of the free surface. If $\eta(\xi)$ is odd then the bottom profile is in general asymmetric.

Assuming that the disturbance to the free surface is small, $|\eta| \ll 1$, (3.10) can be linearised via (3.1) and (3.2) to obtain the approximate formula:

$$\theta_b(\xi) = \text{Im}[-F^{-2}\eta(\xi + i\pi) + i\pi\eta_{\xi}(\xi + i\pi)]. \quad (3.11)$$

The usual dispersion relation for small amplitude gravity waves over a flat bottom in water of finite depth can then be recovered by inserting $\eta = \cos k\phi$ into (3.11). This yields

$$\theta_b(\phi) = \left(\frac{1}{F^2} \tanh k - k \right) \cosh k \sin k\phi. \quad (3.12)$$

Setting $\theta_b \equiv 0$ and assuming that the bracketed term vanishes, we obtain the dimensionless form of the expected linear dispersion relation $F^2 = k^{-1} \tanh k$ [e.g. 14] Since $k^{-1} \tanh k < 1$ for $k > 0$ this dispersion relation holds when $F < 1$, corresponding to subcritical flow. If the bracketed term does not vanish then (3.12) provides the solution for a bottom with small amplitude sinusoidal corrugations of wave number k for general Froude number F .

4. Results

In what follows the surface displacement function, $\eta(\xi)$, is taken to be known. We justify assuming that the surface data is provided in this format by appealing to the commonly adopted rule-of-thumb approximation that $x \approx \phi$ for these type of flows. The validity of this approximation will be discussed below. The bottom angle, $\theta_b(\xi)$, can then be computed from the exact formula (3.10), and the bottom profile, $y_b(\xi)$, can be found by integrating the second relation in (3.3). This requires knowledge of the flow speed at the bottom, and hence of τ_b . We may calculate this in terms of known values using the explicit formula [e.g. 11],

$$\tau_b(\phi) = \int_{-\infty}^{\infty} \frac{\theta_f(\phi')}{1 + e^{\pi(\phi - \phi')}} d\phi' - \int_{-\infty}^{\infty} \frac{\theta_b(\phi')}{1 - e^{\pi(\phi - \phi')}} d\phi', \quad (4.1)$$

but on the truncated domain $-L \leq \phi \leq L$, for some sufficiently large L . In practice (3.3) is integrated forwards from $\phi = -L$ using the trapezium rule. In the following subsections we consider a number of different surface profiles to illustrate the use of the exact formula. In places we will compare the present results with those obtained using the TSVD approach of Robbins *et al.* [11]. In the latter method a numerical approximation to the bottom angle $\theta_b(\xi)$ is obtained by discretizing the integral equation (2.5) (written in a slightly different format) to reduce the problem to the inversion of a linear matrix system of algebraic equations. Since the matrix is singular in the limit as the discretization length is taken to zero, the problem is regularized and a numerical solution constructed by first truncating the set of singular values to remove those close to zero. A full description of the method can be found in Robbins *et al.* [11] (see also Robbins [10]).

In the results presented in the following section, typically we impose the surface disturbance $\eta(\xi)$, and deduce the bottom angle $\theta_b(\xi)$ using (3.10). These results have been checked by confirming numerically that if we substitute $\theta_f(\xi)$ and $\theta_b(\xi)$ into (2.5) then we recover the expected value for $\tau_f(\xi)$ in agreement with that provided by (3.1).

4.1. Gaussian surface displacement

We begin with the case of a elevated Gaussian surface profile for which

$$\eta(\xi) = ae^{-(\beta\xi)^2} = ae^{-(\beta\xi)^2/\pi^2}, \quad (4.2)$$

where the constants $a > 0$ and $\beta > 0$ represent the amplitude and breadth of the free surface displacement, respectively. The exact solution (3.10) holds provided that $\tau_f(\xi)$ and $\theta_f(\xi)$ are analytic in the complex strip \mathcal{D} . According to (3.1), $\tau_f(\xi)$ has singularities in the complex ξ plane at points where

$$\eta = \frac{F^2}{2}. \quad (4.3)$$

Assuming that $a \leq F^2/2$, singularities arise on the imaginary axis at $\xi = \pm i\xi_0$, where ξ_0 is real and given by

$$\xi_0 = \frac{\pi}{\beta} \left(\ln \frac{F^2}{2a} \right)^{1/2} > 0. \quad (4.4)$$

Evidently the singularities enter \mathcal{D} when $|\xi_0| = \pi$, that is when $a = a_0$ with

$$a_0 \equiv \frac{F^2}{2} e^{-\beta^2}. \quad (4.5)$$

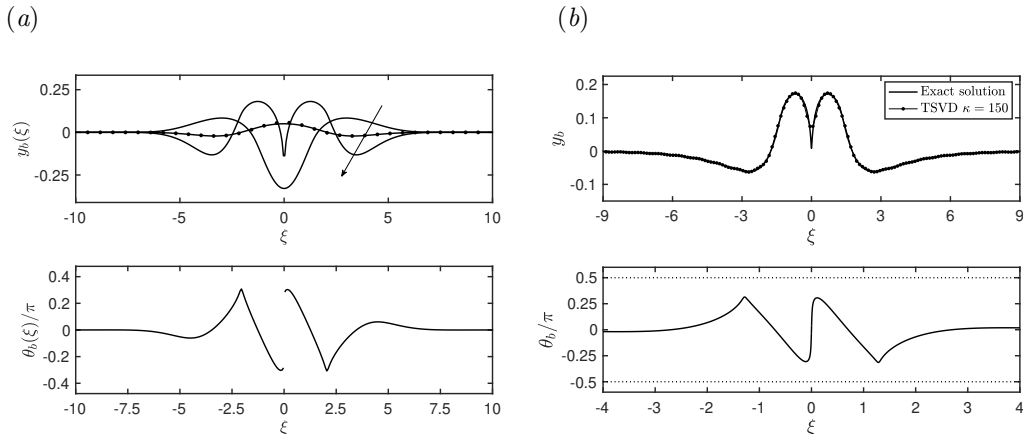


Figure 2: (a) Profiles $y_b(\xi)$ and $\theta_b(\xi)$ for the Gaussian free surface (4.2) with $\beta = 1.0$, $F = 1.1$, and $a = 0.223 (= a_0)$, 0.038 and -0.150 (top panel - the arrow indicates the direction of a increasing). The marker points in the top panel correspond to the linearised formula (3.11). The bottom panel shows $\theta_b(\xi)/\pi$ for the extreme case $a = a_0 = 0.265$. It undergoes a jump discontinuity at $\xi = 0$. (b) $y_b(\xi)$ and $\theta_b(\xi)$ for the sech^2 profile (4.8) with $a = 0.175$, $\beta = 1.0$ and $F = 1.1$. The blue broken curve in the upper panel is the solution produced by the truncated TSVD method on the domain $\xi \in [-10\pi, 10\pi]$ with $N_f = N_b = 500$ and truncation level $\kappa = 150$.

This imposes the upper bound condition $a \leq a_0$ on the surface disturbance amplitude. When this critical surface amplitude is attained the bottom response y_b has a acute-angled corner at $\xi = 0$ where the flow has a stagnation point.

Fig. 2(a) shows computed topographies for a range of surface amplitudes when $\beta = 1.0$ and $F = 1.1$. The prediction of the linearised formula (3.11) with $a = 0.038$ is shown in the top panel with marker points, and it can be seen to almost coincide with the corresponding fully nonlinear result. The corner angle in the extreme case $a = a_0$ can be deduced directly from (3.10). The corner apex corresponds to the branch point of the logarithm in τ_f , which is located at $\xi = i\pi$. Near to this point $\tau_f \sim (1/2) \ln w$, where $w = \xi - i\pi$. Accordingly, in (3.10) $\text{Im}[\tau_f(\xi + i\pi)]$ jumps by $\pi/2$ as real valued ξ passes through zero. The θ_f term in (3.10) varies continuously through the branch point, and hence there is overall a jump in θ_b of $\pi/2$ making the corner angle 90° . Since this argument is independent of the functional form of the surface profile, its conclusion should be generic. Bottom profiles for larger surface amplitudes with $a > a_0$ are unphysical as y_b diverges at $\xi = 0$.

If τ_f is singular at some point then θ_f will be singular at the same point owing to the interdependence of these two functions through (3.2). However, a further singularity may arise from the arcsin that is introduced by inverting (3.2) to obtain θ_f . In particular, using the well known logarithmic formula for arcsin we have

$$\theta_f = i \ln\left(\sqrt{1 - \zeta^2} - i\zeta\right), \quad (4.6)$$

where

$$\zeta \equiv \pi\eta\xi e^{\tau_f} = 2\left(\frac{a^2\beta^4}{\pi^2}\right)^{1/2} \xi e^{-\beta^2\xi^2/\pi^2} \left(1 - \frac{2a}{F^2} e^{-\beta^2\xi^2/\pi^2}\right)^{1/2}. \quad (4.7)$$

Evidently $\sqrt{1 - \zeta^2} \neq i\zeta$ for any complex ζ , but there remains the possibility of a square-root branch point singularity in (4.6) at the location in the complex ξ plane where $\zeta^2 = 1$. By solving the latter equation numerically using Newton's method for the

case in Fig. 2(a) when $a = a_0$, we find that θ_f has singularities just outside of \mathcal{D} at $\xi = \pm 2.06 + 3.18i$ (and their reflections in the lower half plane). The presence of these singularities close to the boundary of \mathcal{D} accounts for the sharp (but continuous) variations in the extreme θ_b profile at $\xi \approx \pm 2.1$ shown in the lower panel of Fig. 2(a).

4.2. sech^2 surface displacement

As a second example we consider the surface displacement profile

$$\eta(\xi) = a \text{sech}^2(\beta\xi/\pi), \quad (4.8)$$

where a and $\beta > 0$ are constants. Condition (4.3) implies that there are τ_f singularities in \mathcal{D} on the real axis if $a > F^2/2$. If $0 < a < F^2/2$ then the τ_f singularities lie on the imaginary axis at $\xi = \pm\xi_1 i$, where

$$\xi_1 = \frac{\pi}{\beta} \cos^{-1}\left(\sqrt{\frac{2a}{F^2}}\right). \quad (4.9)$$

They are inside \mathcal{D} if $(F^2/2)\cos^2\beta < a < F^2/2$. If $a < 0$ the τ_f singularities lie in \mathcal{D} if and only if $\beta > \pi/2$. A sample calculation is presented in Fig. 2(b) for the case $a = 0.175$, $\beta = 1.0$ and $F = 1.1$. Shown together with the exact solution in the top panel is the numerical approximation computed using the TSVD method of Robbins *et al.* [11] with $N_f = N_b = 500$ collocation points on the free surface (N_f) and on the bottom (N_b) over the computational domain $\xi \in [-10\pi, 10\pi]$. In the TSVD method the singular values arising from the singular value decomposition are first ordered and then the κ smallest values are arbitrarily set to zero to mitigate issues with ill-conditioning. The rationale for choosing κ is discussed at length by Robbins [10]. For the calculation in Fig. 2(b) the value $\kappa = 150$ was chosen. In this example the closest τ_f and θ_f singularities are located just outside of \mathcal{D} at $\xi = \pm 3.151i$ and at $\xi = \pm 1.292 + 3.166i$ (with reflections of the latter in the lower half plane), respectively. Consequently, the bottom angle is almost discontinuous at $\xi = 0$ and it develops a rapid change in slope around $\xi = \pm 1.29$. The bottom profile from the exact solution and that from the TSVD are rather close over the entire computational domain. The computational parameters for the TSVD have been chosen by trial and error to give the smoothest profile that is free from oscillations away from the obstacle; notably the domain size needs to be taken to be sufficiently large. TSVD computations on a narrower domain capture the profile over much of the domain but do not accurately reproduce the slope discontinuity at $\xi = 0$.

4.3. Witch of Agnesi surface displacement

Next we consider a disturbance to the free surface in the form of a witch of Agnesi curve with

$$\eta(\xi) = \frac{a}{1 + \beta^2\xi^2/\pi^2} \quad (4.10)$$

for constants a, β . Evidently η has a singularity at $\xi = \pm\xi^*$, where $\xi^* = i\pi/\beta$, and it lies in \mathcal{D} if $\beta \geq 1$. Condition (4.3) holds for a singularity in τ_f at $\xi = \pm\xi_2 i$ with

$$\xi_2 = \frac{\pi}{\beta} \left(1 - \frac{2a}{F^2}\right)^{1/2}. \quad (4.11)$$

This lies outside \mathcal{D} provided that $a < \hat{a}$, where

$$\hat{a} = \frac{F^2}{2}(1 - \beta).$$

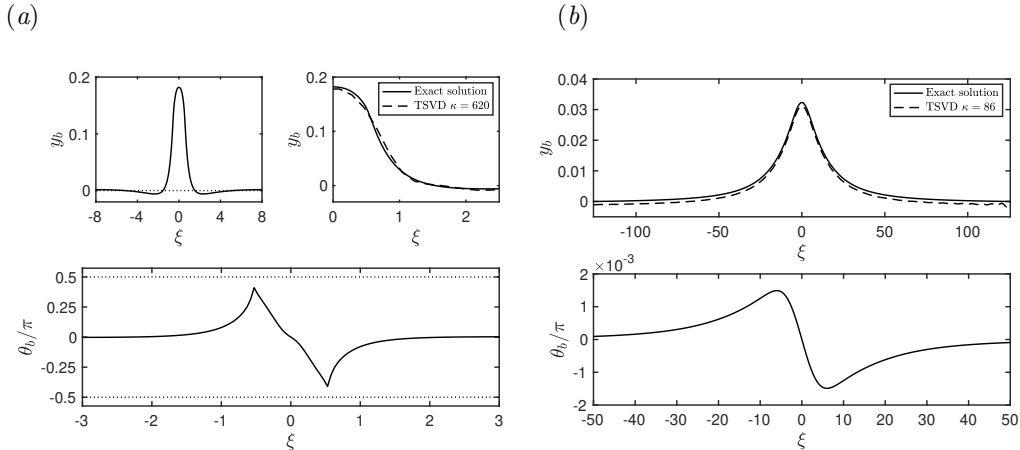


Figure 3: Results for a witch of Agnesi surface disturbance (4.10). (a) The case $a = 0.1$, $\beta = 0.872694738$, and $F = 1.2$. The exact solution for the bottom profile (top panel) is shown with the TSVD computation on the domain $\xi \in [-40\pi, 40\pi]$ with $N_f = N_b = 2080$ and $\kappa = 620$. Also shown is the scaled bottom angle θ_b/π (bottom left panel). The dotted lines in the bottom left panel show $\theta_b = \pm\pi/2$. (b) The case $a = 0.15$, $\beta = 0.25$, and $F = 1.2$. The exact solution for the bottom profile (top panel) is shown together with the TSVD computation carried out on a domain $\xi \in [-40\pi, 40\pi]$ with $N_f = N_b = 501$ and $\kappa = 86$.

The surface angle θ_f has a square-root singularity when $\zeta^2 = 1$, where

$$\zeta = \pi\eta\xi e^{\tau_f} = \frac{2a\beta^2\pi^3\xi}{(\pi^2 + \beta^2\xi^2)^2} \left(1 - \left(\frac{2a}{F^2} \right) \frac{\pi^2}{\pi^2 + \beta^2\xi^2} \right)^{1/2},$$

whose roots satisfy a quintic equation in ξ^2 .

It is of interest to discuss an example for which τ_f is everywhere analytic in \mathcal{D} , but for which θ_f is singular on its boundary. Such an example is shown in Fig. 3(a) for the case $a = 0.1$, $\beta = 0.872694738$ and $F = 1.2$. Here the value of β has been chosen so that θ_f singularities lie at $\xi = \pm(0.54 \pm 3.1415926i)$, with the imaginary part quoted correct to seven decimal places (and there are no other θ_f singularities within \mathcal{D}). In this case $\xi_2 = 3.341$ so that the τ_f singularity lies outside \mathcal{D} . A wide domain is necessary to capture the slow, algebraic far-field decay such that $y_b = O(\xi^{-2})$ and $\theta_b = O(\xi^{-3})$ when $|\xi| \gg 1$, although in Fig. 3(a) we have displayed only a narrowed view close to the origin. The singular behaviour is evident in the lower panel where there are jumps in the slope of the bottom angle θ_b curve at $\xi = \pm 0.53$. From (3.2), and since $\tau_f(\xi)$ is smooth, this implies discontinuities in $d^2y_b/d\xi^2$, and hence the curvature of the bottom profile, at these points. Also shown in the top panel is the TSVD result obtained with $N_f = N_b = 2080$ on the computational domain $\xi \in [-40\pi, 40\pi]$ and with $\kappa = 620$. Despite the curvature singularity, this captures the exact profile fairly well. Fig. 3(b) shows a less challenging example where all of the τ_f and θ_f singularities are located outside \mathcal{D} . In this case the TSVD approach is able to capture the exact bottom profile with far fewer collocation points.

4.4. Physical profiles: negative Gaussian surface

Up to this point we have assumed that the surface profile is given in terms of the velocity potential, $\phi = \xi/\pi$. Since in practice we would have knowledge of $Y_f(x)$ rather than $y_f(\phi)$, and since we are likely to be more interested in $Y_b(x)$ than $y_b(\phi)$, it is relevant to scrutinize how well the one approximates the other. The surface and bottom

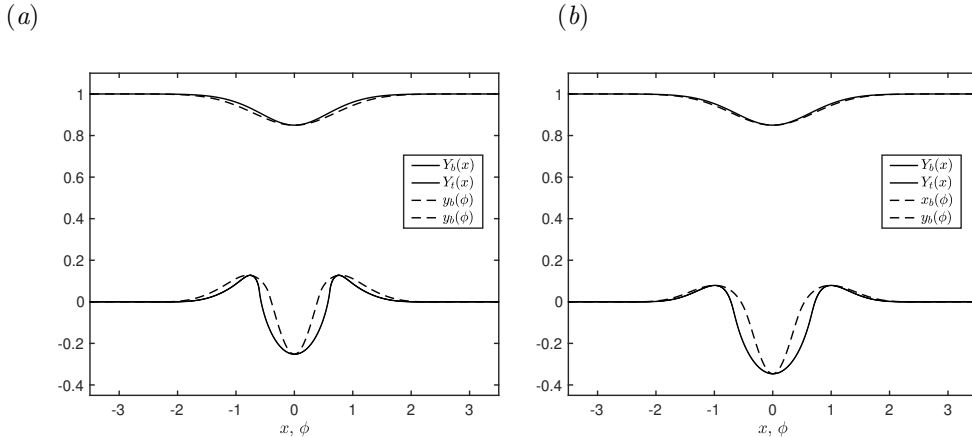


Figure 4: Surface and bottom profiles $y_f(\phi)$ and $y_b(\phi)$, $Y_f(x)$ and $Y_b(x)$ for the imposed Gaussian free surface $Y_f(x) = 1 + \eta(x)$ and η given by (4.2) for $\beta = 1.0$, $a = -0.15$ and (a) the subcritical case $F = 0.8$ and (b) the supercritical case $F = 1.2$. In both (a) and (b) the solid lines correspond to the physical profiles, $Y_f(x)$ and $Y_b(x)$, and the dashed lines correspond to the profiles $y_f(\phi)$ and $y_b(\phi)$.

profiles in physical space, namely $Y_f(x)$ and $Y_b(x)$, are constructed by integrating the pairs of equations in (3.2) and (3.3), the latter using (4.1) to calculate $\tau_b(\phi)$. In Fig. 4 we show calculations for a negative Gaussian surface displacement, given by (4.2), for subcritical flow (panel a) and for supercritical flow (panel b) at sample values of the Froude number and for a moderate-sized displacement to the free surface. When the amplitude is negative, so that $a < 0$ in (4.2), the τ_f singularity is located at

$$\xi = \pm i \frac{\pi}{b} \left(\pm i \pi + \log \left(\frac{F^2}{2|a|} \right) \right)^{1/2}. \quad (4.12)$$

In the subcritical case, the train of waves that typically characterise subcritical flow downstream of an obstacle are absent by design (since the surface profile is imposed this way). This is a flow of type 4 in the nomenclature of Binder *et al.* [5]. The supercritical flow in Fig. 2(b) is of type 1 in the taxonomy of Binder *et al.* [5]. There are no singularities in \mathcal{D} for either the supercritical or the subcritical cases shown in the figure. The solid lines in the two panels show the physical profiles. For the chosen surface amplitudes the physical surface profiles and the approximate ϕ -profiles, shown with the broken lines, are rather close. As expected the discrepancy between the two will worsen as the amplitude, a , is increased. However, it is striking that there is substantial deviation between the physical profiles and the ϕ -profiles on the bottom. Similar observations hold for the other surface profiles considered above.

4.5. Hydraulic fall

We conclude with a discussion of a hydraulic fall, a flow of type 11 in the terminology of Binder *et al.* [5]. For a hydraulic fall the surface level and flow speed are given in dimensional units by H and U downstream (as in Fig. 1), and by h and u upstream. The dynamic boundary condition at the free surface is obtained from Bernoulli's equation. Defining the flow speed ratio $q = u/U$ and the layer depth ratio $d = h/H$, it takes the form

$$1 - q^2 + \frac{2}{F^2}(1 - d) = 0, \quad (4.13)$$

where the Froude number F was defined in (1.1). Mass conservation implies that $qd = 1$, and we may use this to infer the relation for the upstream Froude number,

$$F_u = q^{3/2}F, \quad F_u^2 \equiv \frac{u^2}{gh}. \quad (4.14)$$

We assume without loss of generality that $q < 1$ so that the flow is faster downstream the upstream; and, consequently, the surface level is lower downstream than upstream, so that $d > 1$. Consistent with Forbes [2], if $q > 1$ then (4.13) and (4.14) imply that $F > 1$ and $F_u < 1$ so that the flow is supercritical downstream and subcritical upstream. The symmetry of the governing equations means that, given such a solution, we may reverse the flow direction to obtain another solution for which the surface level is higher downstream than upstream corresponding to a hydraulic rise. However, such a solution is expected to be unstable and, therefore, of limited physical interest.

Substituting $q = 1/d$ into (4.13), and assuming that $d \neq 1$, we obtain the quadratic equation for $\Delta \equiv d - 1$, the dimensionless difference in height between the downstream level and the upstream level,

$$\Delta^2 + \left(2 - \frac{F^2}{2}\right)\Delta + 1 - F^2 = 0. \quad (4.15)$$

The relevant solution is

$$\Delta = \frac{F^2}{4} \left(1 + \left(1 + \frac{8}{F^2}\right)^{1/2}\right) - 1. \quad (4.16)$$

As an illustrative example we impose the surface disturbance

$$\eta(\xi) = \frac{\Delta}{2}(1 - \tanh k\xi) \quad (4.17)$$

for constant $k > 0$, such that $\eta \rightarrow 0$ as $\xi \rightarrow \infty$. The procedure described in the previous sections can be followed to determine the bottom angle θ_b via the exact formula (3.10), and then y_b by integrating the second equation in (3.3).

The surface profile (4.17) is itself singular at $\xi = (2n + 1)\pi i/2k$, for $n = 0, 1, 2, \dots$. These singularities are outside of \mathcal{D} if $k < 1/2$. Fulfilling criterion (4.3) the τ_f singularities for the surface profile (4.17) are located at

$$\xi = \frac{1}{2k} \log\left(1 - \frac{\Delta(2 + \Delta)}{(1 + \Delta)^2}\right) \pm \frac{\pi}{2k}i, \quad (4.18)$$

where we have used (4.15) to eliminate the Froude number as $F^2 = 2(1 + \Delta)^2/(2 + \Delta)$. Evidently these, as well as the η singularity, lie in \mathcal{D} if $k > 1/2$. The singularity associated with the surface angle θ_f occurs where $\zeta(\xi)^2 = 1$, with

$$\zeta = \pi\eta\xi e^{\tau_f} = -\frac{k\pi\Delta}{2} \left(1 - \frac{\Delta}{F^2}(1 - \tanh k\xi)\right)^{1/2} \operatorname{sech}^2 k\xi. \quad (4.19)$$

A typical solution is shown in Fig. 5(a) for the case $k = 0.25$ and $F = 1.2$ (so that $\Delta = 0.282$ according to (4.16)), in which case all of the singularities lie outside of \mathcal{D} . Notice that the bottom profile is asymmetric with respect to ξ .

Turning now to a more realistic example, instead of imposing an artificial surface profile we examine one that is known to be a solution of the full water wave problem (2.1), (2.2), and (2.3) for a prescribed topography. The surface profile $Y_f(x)$ shown in the upper panel of Fig. 5(b) is that corresponding to the hydraulic fall solution to the forwards

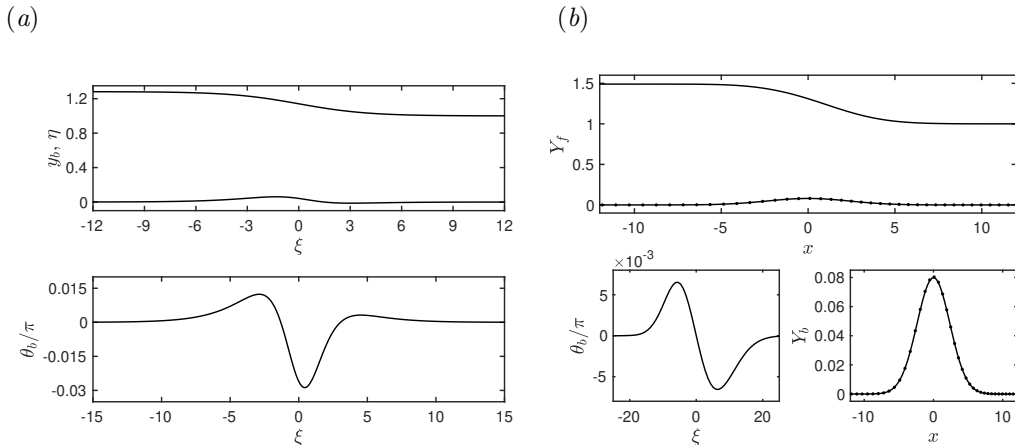


Figure 5: Hydraulic fall solutions: (a) Results for the tanh profile (4.17) with $k = 0.25$, $F = 1.2$ ($\Delta = 0.282$). The upper panel shows the free surface with the inversely found bottom shape, and the bottom profile shows the scaled topography angle $\theta_b(\xi)/\pi$. (b) The top panel shows the numerically computed free surface profile forward solution to the full water wave problem (2.1), (2.2), and (2.3) with $Y_b(x) = 0.080 \exp(-0.090x^2)$ when $F = 1.336$ ($\Delta = 0.490$). The bottom panels show the inversely found scaled bottom angle $\theta_b(\xi)/\pi$ (left) and topography profile $y_b(x)$ (right). The marker points in the bottom right panel show the topography used in the forwards problem.

problem computed for the Gaussian-shaped topography $Y_b(x) = 0.080 \exp(-0.090x^2)$ when $F = 1.336$. This forwards solution is provided in the form of numerical data on a discrete grid in a computation carried out by Dr J. Keeler. The marker points in the bottom right panel of Fig. 5(b) indicate the original topography used in the forwards problem.

The inverse calculation, in which the topography is recovered from the surface profile, $Y_f(x)$, was carried out as follows. First the discrete free surface data $Y_f(x)$, supplied on a grid of x points, was interpolated with a Chebyshev polynomial using the open-source Matlab code Chebfun [17]. Differentiating the interpolant provides the surface angle θ_f via the relation

$$\frac{dY_f}{dx} = \tan \theta_f, \quad (4.20)$$

and (3.1) provides τ_f . Given $\phi(x, y)$ we define the surface velocity potential $\Phi(x) \equiv \phi(x, Y_f(x))$. Differentiating with respect to x , and using (2.4) and (4.20), it follows that

$$\frac{d\Phi}{dx} = \phi_x + \phi_y \frac{dY_f}{dx} = e^{\tau_f} \sec \theta_f. \quad (4.21)$$

This can be integrated to supply $\Phi(x)$ given some initial condition, say $\Phi(0) = 0$. This relation allows us to infer $\tau_f(\xi)$ and $\theta_f(\xi)$, given that $\xi = \pi\phi(x, Y_f) = \pi\Phi(x)$, over a specified grid of ξ points. Chebyshev interpolants of these functions were then used as a basis to construct rational approximations for $\tau_f(\xi)$ and $\theta_f(\xi)$ that could be used for accurate approximation over complex ξ so as to apply the exact formula (3.10). (See Trefethen [18] for a discussion of the benefits of rational approximation for numerical analytic continuation.) The rational approximation was carried out in Chebfun using the AAA algorithm (Nakatsukasa *et al.* [19]). The resulting inversely-computed bottom profile $Y_b(x)$ is shown with a solid line in the bottom right panel of Fig. 5. The close agreement between this curve and the marker points denoting the original topography used in the forwards problem validates the current procedure.

5. Discussion

We have presented an exact solution to the inverse problem for steady flow over topography that supplies the bottom shape given knowledge of the surface profile. The exact solution is straightforward to compute, and we have shown that it can be used to faithfully recover known topographical data, as was demonstrated in the case of a hydraulic fall. As was noted by Robbins [10] and Robbins *et al.* [11], the problem to recover the bottom shape is linear provided that the surface profile is given as a function of the velocity potential. In the more physically realistic scenario when the surface data is given as a function of the horizontal coordinate, the problem is non-linear, owing to the nonlinear relation between x and ϕ given in (3.2). However, even for moderate-sized surface disturbances $x \approx \phi$ on the surface and the solution to the linear problem provides a good approximation to the physical solution. The discrepancy between the physical profile and the ϕ -profile is much more pronounced at the bottom, but the shift between the two is done in the post-processing and so this does not affect the linearity of the formulation.

We have compared our results with those found using the numerical Truncated Singular Value Decomposition (TSVD) method adopted by Robbins *et al.* [11]. In doing so we have confirmed the accuracy of this computational approach while emphasising the importance of choosing the computational parameters carefully. In particular we found that a carefully performed computation was able to accurately reproduce bottom topographies featuring a slope discontinuity and a discontinuity in the curvature.

Inverse problems are well known to be ill-posed in general. Our problem formulation involves a Stieltjes integral equation, which is an example of a Fredholm integral equation of the first kind, and these are also well known to be ill-posed. The TSVD method of Robbins *et al.* [11], which works with essentially the same integral equation formulation as ours, regularizes the problem by removing singular values that are deemed too close to zero. Here, however, we have an exact solution to the problem, and so the question arises of how the ill-posedness manifests itself in the present approach. The answer lies in the analytical continuation that is necessary to extend the definition of the surface data off the real line and into the complex plane. Analytic continuation is well known to be unique but ill-posed (e.g. Trefethen [20]). Therefore, in keeping with the expectation that the solution to the Stieltjes equation does not depend continuously on the input data, we expect that small perturbations to the free surface will result in large changes to the bottom topography. To illustrate this we consider the perturbed Gaussian surface displacement,

$$\eta(\xi) = ae^{-(\beta\xi)^2/\pi^2}(1 + \epsilon \cos(k\xi/\pi)), \quad (5.1)$$

setting $a = 0.1$ and $\beta = 1.0$. In Fig. 6 we plot the corresponding bottom profiles $y_b(\xi)$ for the undisturbed surface with $\epsilon = 0$ and for the disturbed surface with $\epsilon = 0.004$ and $k = 5.0$ for the subcritical and supercritical Froude numbers $F = 0.85$ and $F = 1.2$. Evidently, there is a strong sensitivity to a small change in ϵ , this being particularly pronounced for the subcritical case. This sensitivity increases as the perturbation wave number k is increased.

Of course in practice the functional form of the surface profile is not known for experimental data. Although this can be handled using the TSVD approach of Robbins *et al.* [11] (and, indeed, those authors accounted for the possibility of noisy data), it is nevertheless of interest to adapt the present approach to such data. A step in this direction has been taken here by reproducing the bottom profile for a hydraulic fall using discrete numerical data obtained from a solution to the full forwards problem. This was done by constructing a rational approximation to the real surface values, and then extending its definition into the complex plane to infer values along the edge of

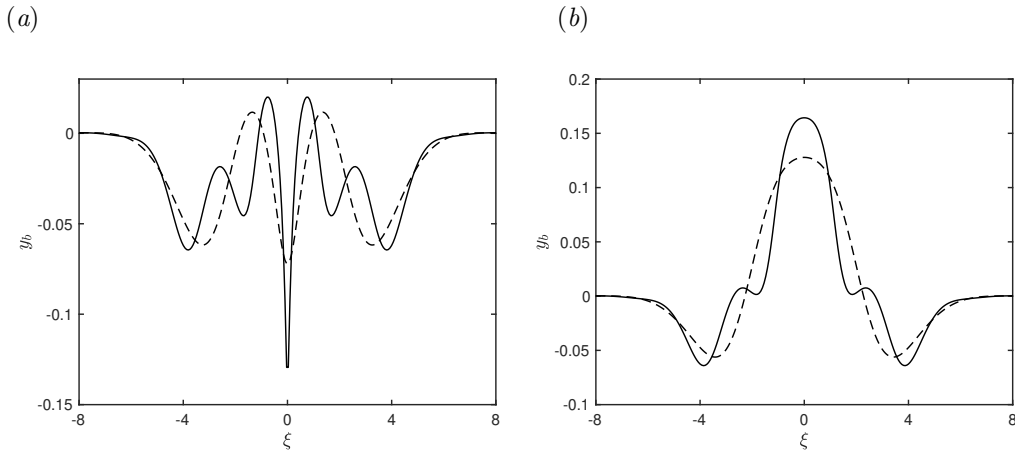


Figure 6: Sensitivity of the topography to small surface perturbations. The bottom profile $y_b(\xi)$ corresponding to the surface shape (5.1) when $\epsilon = 0$ (dashed lines) and $\epsilon = 0.004$, $k = 5.0$ (solid lines): (a) $F = 0.85$, and (b) $F = 1.2$. The surface shape parameters are $a = 0.1$ and $\beta = 1.0$.

the strip \mathcal{D} . In general, however, the extension of such rational approximations is not a straightforward task and, in particular, attempting to locate singularities in the complex plane, as is required here in the use of (3.10), is frustrated by difficulties such as the possible presence of Froissart doubles (spurious poles); see Trefethen [18] and Nakatsukasa *et al.* [19] for a discussion.

Finally we remark that in the case of still water it is obvious that any bottom profile is consistent with a flat free surface, and this suggests some degeneracy in the inverse problem for which the solution is unique in the presence of a flow. The limit of still water is reached by taking $F \rightarrow 0$, in which case it is appropriate to rescale the surface deflection and surface angle by writing $\eta = F^2 f(\xi)$ and $\theta_f = F^2 \Theta(\xi)$, for some f and Θ , which are both of order unity. The exact solution (3.10) yields the leading order approximation to the bottom angle,

$$\theta_b(\xi) = \frac{1}{2} \arg\left(1 - f(\xi + i\pi)\right). \quad (5.2)$$

Notably the bottom angle is of order unity. For the Gaussian surface deflection (4.2), a smooth bottom angle is obtained provided that

$$-\frac{F^2}{2} e^{(\pi^2/4 - 1)\beta^2} \leq \eta(0) \leq \frac{F^2}{2} e^{-\beta^2}. \quad (5.3)$$

Thus in the limit of still water, $F \rightarrow 0$, an arbitrary bottom profile will correspond to a surface deflection that is sandwiched inside a ‘boundary-layer’ of thickness $O(F^2)$ about the flat free surface. In this sense the infinitude of inverse solutions for a flat free surface in still water represents a singular limit of the present problem.

Acknowledgement

The author wishes to thank Dr Jack Keeler and Dr Connor Robbins for kindly providing the surface data for the hydraulic fall calculation and the code to compute the TSVD solutions, respectively. The author is grateful to the anonymous referees for insightful comments that helped to improve the manuscript.

Conflict of Interest Statement

The author reports no conflict of interest.

Data availability

The data generated and/or analysed during the current study are available from the corresponding author on reasonable request.

References

- [1] L. K. Forbes, L. W. Schwartz, Free-surface flow over a semicircular obstruction, *J. Fluid Mech.* 114 (1982) 299–314.
- [2] L. K. Forbes, Critical free-surface flow over a semi-circular obstruction, *J. Eng. Math.* 22 (1) (1988) 3–13.
- [3] F. Dias, J.-M. Vanden-Broeck, Open channel flows with submerged obstructions, *J. Fluid Mech.* 206 (1989) 155–170.
- [4] A. C. King, M. I. G. Bloor, Free-surface flow of a stream obstructed by an arbitrary bed topography, *Quart. J. Mech. Appl. Math.* 43 (1) (1990) 87–106.
- [5] B. J. Binder, M. G. Blyth, S. W. McCue, Free-surface flow past arbitrary topography and an inverse approach for wave-free solutions, *IMA J. Appl. Math.* 78 (4) (2013) 685–696.
- [6] E. O. Tuck, On air flow over free surfaces of stationary water, *ANZIAM J.* 19 (1) (1975) 66–80.
- [7] M. Sellier, Inverse problems in free surface flows: a review, *Acta Mech.* 227 (3) (2016) 913–935.
- [8] F. Chardard, F. Dias, H. Y. Nguyen, J.-M. Vanden-Broeck, Stability of some stationary solutions to the forced KdV equation with one or two bumps, *J. Eng. Math.* 70 (1) (2011) 175–189.
- [9] N. S. Abdelrahman, M. S. Abou-Dina, A. F. Ghaleb, Free-surface, wave-free gravity flow of an inviscid, incompressible fluid over a topography: an inverse problem, *Z. Angew Math. Phys.* 72 (6) (2021) 1–12.
- [10] C. Robbins, Free surface flow over topography: an inverse approach, Ph.D. thesis, University of East Anglia (2021).
- [11] C. Robbins, M. G. Blyth, J. Maclean, B. J. Binder, A method to calculate inverse solutions for steady open channel free-surface flow, *J. Fluid Mech.* 977 (2023) A46.
- [12] E. C. Titchmarsh, *Introduction to the theory of Fourier integrals*, Oxford: The Clarendon Press, 1948.
- [13] J. Neal, L. Hawker, J. Savage, M. Durand, P. Bates, C. Sampson, Estimating river channel bathymetry in large scale flood inundation models, *Water Res. Res.* 57 (5) (2021) e2020WR028301.
- [14] J. J. Stoker, *Water waves: The mathematical theory with applications*, Vol. 36, John Wiley & Sons, 1957.

- [15] H. Bateman, A. Erdélyi, W. Magnus, F. Oberhettinger, Tables of integral transforms, Vol. 1, McGraw-Hill New York, 1954.
- [16] M. A. Ablowitz, P. A. Clarkson, Solitons, nonlinear evolution equations and inverse scattering, Vol. 149, Cambridge University Press, 1991.
- [17] T. A. Driscoll, N. Hale, L. N. Trefethen, Chebfun guide. <https://www.chebfun.org>. (2014).
- [18] L. N. Trefethen, Approximation Theory and Approximation Practice, Extended Edition, SIAM, 2019.
- [19] Y. Nakatsukasa, O. Sète, L. N. Trefethen, The AAA algorithm for rational approximation, SIAM J. Sci. Comp. 40 (3) (2018) A1494–A1522.
- [20] L. N. Trefethen, Quantifying the ill-conditioning of analytic continuation, BIT Num. Math. 60 (4) (2020) 901–915.